PCCP

PAPER

Cite this: *Phys. Chem. Chem. Phys.*, 2015, **17**, 29079

Electric-dipole effect of defects on the energy band alignment of rutile and anatase TiO_2

Daoyu Zhang,[a] Minnan Yang[b] and Shuai Dong*[a]

Received 30th July 2015,
Accepted 5th October 2015

DOI: 10.1039/c5cp04495b

www.rsc.org/pccp

Titanium dioxide materials have been studied intensively and extensively for photocatalytic applications. A long-standing open question is the energy band alignment of rutile and anatase TiO_2 phases, which can affect the photocatalytic process in the composite system. There are basically two contradictory viewpoints about the alignment of these two TiO_2 phases supported by the respective experiments: (1) straddling type and (2) staggered type. In this work, our DFT plus *U* calculations show that the perfect rutile(110) and anatase(101) surfaces have the straddling type band alignment, whereas the surfaces with defects can turn the band alignment into the staggered type. The electric dipoles induced by defects are responsible for the reversal of band alignment. Thus the defects introduced during the preparation and post-treatment processes of materials are probably the answer to the above open question regarding the band alignment, which can be considered in real practice to tune the photocatalytic activity of materials.

I. Introduction

The discovery of water photolysis on the TiO_2 electrode by Fujishima and Honda[1] has evoked an enormous amount of investigations on TiO_2.[2] During the past four decades, a wealth of information related to the photocatalytic properties of TiO_2, as well as other physical and chemical properties, has been collected.[3,4] Rutile and anatase are the two principal crystalline phases of TiO_2 quite suitable for photocatalytic applications. It is widely assumed that the anatase phase TiO_2 displays higher photocatalytic activity compared to the rutile one, because anatase materials have lower rates of recombination of electron–hole pairs.

Most interestingly, the composite consisting of anatase and rutile TiO_2 exhibits even higher photocatalytic activity than individual components due to the synergistic effect from the separation of excited electrons and holes at the interface between the anatase and rutile phases.[5–10] A number of previous experimental studies were devoted to probing the migration direction of carriers at the interface. However, two opposite results have been obtained: (1) electrons transfer from anatase to rutile[11–13] and (2) electrons transfer from rutile to anatase.[14–17]

The debate on this charge migration also took place in the theoretical aspect. The effective separation of the photoexcited electron–hole pairs at the interface is supposed to be the result of the energy difference in band edges of anatase and rutile. Two types of band alignments of anatase and rutile phases were predicted by using different theoretical methods, leading to electron transfer in two opposite directions, as illustrated in Fig. 1. The straddling type (Fig. 1(a)) is characterized by band edges of anatase straddling those of rutile, which will drive the migration of both electrons and holes from anatase to rutile.[18] For the staggered type (Fig. 1(b)), the band edges of anatase are

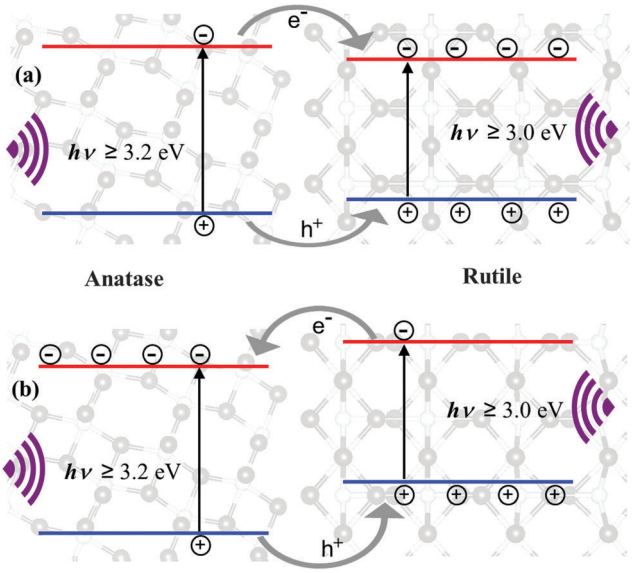

Fig. 1 The proposed two types of band alignment between rutile and anatase TiO_2: (a) the straddling type, in which excited electrons and holes will prefer to accumulate in the rutile phase and (b) the staggered type, in which the excited electrons prefer to migrate to the conduction band of the anatase, while the holes prefer to move to the valence band of the rutile.

[a] *Department of Physics & Jiangsu Key Laboratory for Advanced Metallic Materials, Southeast University, Nanjing, 211189, China. E-mail: sdong@seu.edu.cn*
[b] *Department of Physics, China Pharmaceutical University, Nanjing, 211198, China*

lower than those of rutile, leading to the inverse migration of electrons/holes.[17,19–21]

To date, the scenario of carrier transfer process in the mixed-phase TiO_2 composite remains ambiguous, which severely influences the correct design of the mixed-phase TiO_2 to improve the photocatalytic activity of this material. Therefore, it is important and useful to figure out the real mechanisms, even partial, involved in the band alignment of rutile and anatase TiO_2.

At the interface between two semiconductors, many factors, such as the charge transfer across the interface, dangling bonds, atomic arrangements at the interface, charge trapping sites, interfacial tension, and the interfacial orbital reconstruction, influence the energy band alignment of the heterostructure,[20,22–24] so it is difficult to extract the required information of the effect of the electric dipole just induced by the interfacial defects on the band alignment. Thus, the model of the interface between two TiO_2 phases is not suitable to act as the calculation method for achieving the aim of this research.

To clearly understand the electric dipole effect of defects on the band alignment of rutile and anatase TiO_2, we carry out computational analyses separately on the two phases, obtaining their absolute band energies and band alignment. The difference estimated in this way between conduction band edges of two TiO_2 phases, namely the band offsets, is the Schottky limit value. The Schottky limit is an important parameter that acts as the boundary condition imposed on a particular interface, and one can provide just corrections to the Schottky limit to get the band offsets of the real heterostructure. In this sense, in the following, the discussion on the transfer of the photoexcited carriers is based on the Schottky limit.

Our previous studies[25,26] and studies by other groups[27,28] predicted that the electric dipoles created by chemisorbed molecules or atoms on the surface of a semiconductor can significantly change the band-edge energies. Based on this idea, in the present work, the bridging oxygen vacancies (O-vac's) and the hydroxyl groups (O–H's), which can be introduced into the TiO_2 surfaces during the material preparation, are studied to verify the effect of electric dipoles on the band alignment of rutile and anatase TiO_2.

II. Model & method

First-principles calculations were performed using the projector-augmented wave (PAW) pseudopotentials as implemented in the Vienna ab initio Simulation Package (VASP).[29,30] The Perdew–Burke–Ernzerhof (PBE) GGA exchange–correlation functional was used. The Hubbard-type correction (U) within Dudarev's approximation[31] was applied to strongly localize Ti 3d orbitals for remedying on-site Coulomb interactions. The energy cutoff for the plane wave basis set was set to 450 eV and the convergence criteria in energy were 10^{-5} eV. The atomic positions were relaxed towards equilibrium using the conjugate gradient method until the force on each atom is less than 0.01 eV $Å^{-1}$. Gaussian smearing with a width of 0.01 eV was employed for calculating partial occupancies.

The stoichiometric $p(3 \times 2)$ rutile $TiO_2(110)$ and $p(1 \times 3)$ anatase $TiO_2(101)$ supercell surfaces were built from experimental lattice parameters. The two supercells have the same number of 144 atoms, half of which are fixed at their bulk positions during the relaxation process, as indicated in Fig. 2(a) and (b). The number of two-fold bridging O atoms and five-fold bridging Ti atoms are also the same at these two surfaces, beneficial to compare the following calculated results of the two surfaces. In real materials, these two surfaces are also the most stable and common ones.[32] A vacuum space of about 11 Å

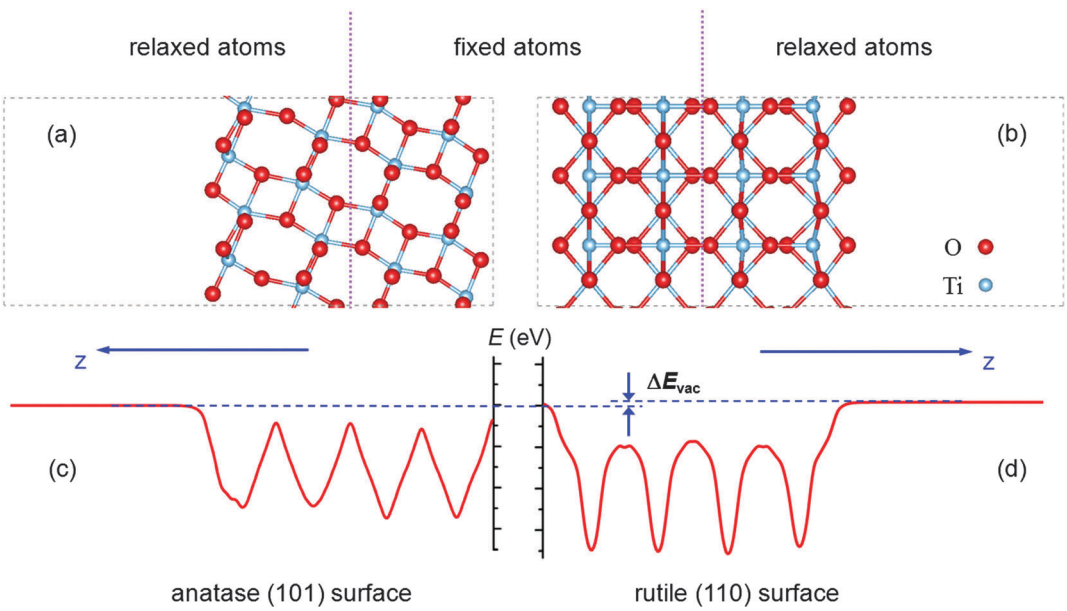

Fig. 2 The surface models of (a) anatase(101) and (b) rutile(110), both of which possess the same number of two-fold bridging O atoms and five-fold bridging Ti atoms. The sketch of (x,y)-planar averaged electrostatic potential for a pair of (c) anatase(101) and (d) rutile(110) surfaces.

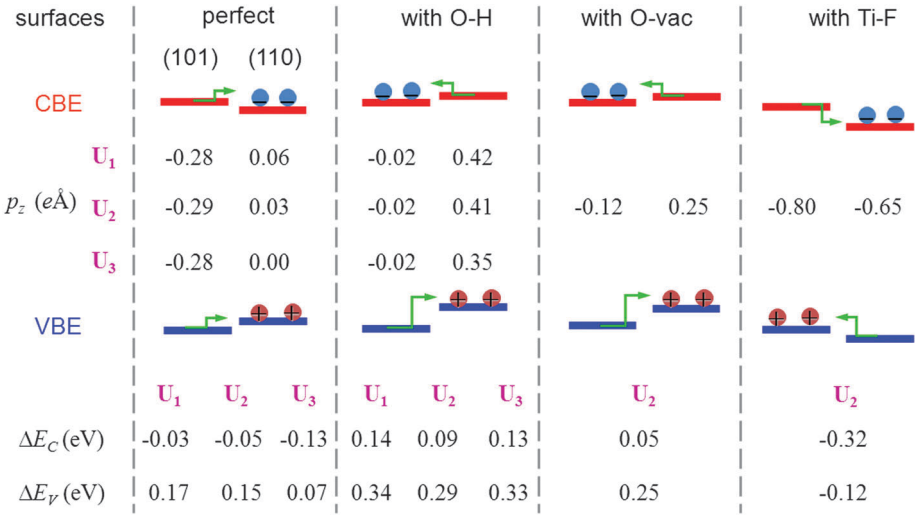

Fig. 3 The DFT+U calculated relative band edges of the clean surfaces and surfaces with defects of O–H, O-vac, and Ti–F. CBE (VBE) denotes the conduction (valence) band edge and ΔE_C (ΔE_V) is the difference in the conduction (valence) band edges between the rutile(110) and anatase(101) surfaces. p_z denotes the z component (perpendicular to the surface) of the electric dipole moment of the surface. The positive value of p_z means that its direction is pointing away from the surface. Here U_1 = 3.3 eV; U_2 = 4.3 eV; and U_3 = 5.3 eV.

was set for the separation of the surface slab from its periodic images. In the direction perpendicular to the slab, the monopole, dipole, and quadrupole corrections have been applied to the electrostatic interaction between the slab and its periodic images. Γ-point-only sampling was used for the geometrical relaxation of surfaces. Automatically generated Γ-point-centered 3 × 2 × 1 (rutile) and 2 × 2 × 1 (anatase) Monkhorst–Pack meshes were used for static electronic structure calculations.

According to previous literature, there are several approaches to align band energy such as the vacuum level alignment, the charge neutrality level alignment, the common anion rule, and so on.[33,34] Although the band alignment deduced from the interface supercell model can reveal accurate values for the band offsets,[35] here the surface model using the vacuum level as a common energy reference is selected. This choice can obtain the relative values between band edges of rutile and anatase and effectively reduce the inaccuracy of the offsets.[36] In detail, the strategy for the band alignment of the corresponding anatase and rutile surfaces is the following. First, based on the (x,y)-planar average electrostatic potential,[21] the difference in the deep vacuum space between the pair of surfaces is calculated as $\Delta E_{vac} = E_{vac}$(rutile) − E_{vac}(anatase). Second, the Kohn–Sham valence band edges from the DFT+U calculations are aligned by subtracting ΔE_{vac}. Third, the conduction band edges are aligned based on the above aligned valence band edges by adding the commonly accepted band gaps of anatase (3.2 eV) and rutile (3.0 eV) TiO_2.[37]

III. Results & discussion

First, we focus on the clean surfaces. Our DFT+U calculations show that the stoichiometric rutile(110) surface is almost non-polar with the very small dipole moment of only ∼0.03 e Å, while the stoichiometric anatase(101) is highly polar with a distinct moment of ∼0.29 e Å independent of the value of U (as listed in the second column of Fig. 3). This electric dipole occurring at the anatase(101) surface is helpful to separate the photogenerated electron–hole pairs and block the electron–hole recombination. The direction of the electric dipole moment from the surface to the inner side implies that photogenerated holes will gather at the surface while electrons will migrate to the inner side. This intrinsic electric dipole at the polar anatase(101) surface may be the reason for mitigating the rates of recombination and back-reaction compared with the rutile phase TiO_2.[38–40] As a consequence, anatase phase TiO_2 displays better photocatalytic activity.

The second column of Fig. 3 shows the energy band alignment for the clean surfaces of anatase and rutile phases. The conduction and valence band edges of the anatase(101) surface straddle those of the rutile(110) surface, in agreement with the calculated results of a quantum-dot supercell composed of the anatase and rutile pair.[18] In the case of the straddling type, excess electrons and holes resulting from irradiation will accumulate in the conduction band and the valence band of rutile TiO_2, respectively, provided anatase and rutile are kept in close contact with each other. Because rutile TiO_2 exhibits high rates of recombination,[41] the accumulated electrons and holes may quickly recombine with each other before they move to the reactants adsorbed onto the surfaces, thus the photocatalytic activity of mixed anatase and rutile phases would be expected to be less efficient with the straddling type alignment. In this sense, the mixed-phase TiO_2 materials free of defects are not advantageous for photocatalytic applications.

In fact, TiO_2 materials always have defects, depending on the preparation conditions and the post-treatment processes. When sputtered and annealed in ultra-high vacuum or bombarded with electrons, TiO_2 samples will lose some bridging oxygen

atoms forming oxygen vacancies (O-vacs).[32] When treated in an atmosphere containing hydrogen, they are ready to combine with hydrogen atoms forming hydroxyl groups (O–Hs).[42,43] The energy band alignment between the anatase(101) and rutile(110) surfaces with the O–H and O-vac coverage of 1/6th monolayer is shown in the third and fourth columns of Fig. 3, respectively. Such a pair of surfaces with equivalent defects has the band alignment of staggered type, independent of the value of U. The switch of the band alignment type from the straddling type to the staggered one indicates that the effect of defects plays a crucial role in tuning the band alignment and thus the photocatalytic activity of two TiO_2 phases and their composition.

The effect of the defects on the band alignment is related to the electric dipoles introduced by defects themselves. Previous studies had demonstrated that the chemisorbed functional groups on semiconductors can supply excess electric dipoles, which change electron energies in semiconductors and shift their whole energy bands together.[26,28] And the energetic variation of electrons in a semiconductor ΔE_{dip} can be formulated within the parallel-plate capacitor approximation as

$$\Delta E_{dip} = e\frac{\Delta p_z}{A\varepsilon\varepsilon_0} \quad (1)$$

where A is the surface area, ε is the effective dielectric constant of the surface layer, and Δp_z is the electric dipole moment induced by functional groups. ε_0 is the dielectric constant of vacuum and e is the elementary charge. Electron energies vary linearly with Δp_z. The defects of O–Hs (O-vacs) bring forth the dipole moments of 0.38 e Å (0.22 e Å) and 0.27 e Å (0.17 e Å) for the rutile(110) and anatase(101) surfaces respectively. In other words, the rutile(110) surface with defects has a larger Δp_z than the anatase(101) surface with the "identical" defects, thus Δp_z increases electron energies in the former more than that in the latter. Even more possibly, the conduction band edge of the rutile(110) surface would surpass that of the anatase(101) surface, such as our cases studied here.

Why do the rutile(110) and anatase(101) TiO_2 phases with the same defect coverage possess different Δp_z values? The case with the same hydroxyl coverage (1/6 monolayer) will be taken as an example to reveal the underlying physical mechanism. First, the Bader charges[44] on H and O atoms of the hydroxyl groups at the anatase(101) and rutile(110) surfaces are almost identical. The difference in charges on H(O) atoms at the two surfaces is only 0.0001 (0.0351) e, whose contribution to Δp_z is negligible. Second, the bond lengths of O–Hs at the two surfaces are identical, being 0.968 Å. Third, according to previous studies, the intrinsic electric dipole of the adsorbed hydroxyl groups itself plays a dominant role in the shift of the band edges of TiO_2 with respect to the polaronic dipole created by structural distortion and charge rearrangement.[25] Thus, one can infer that the different configurations of the hydroxyl groups at the two surfaces are responsible for their different Δp_z values. As shown in Fig. 4, the hydroxyl group at the relaxed rutile(110) surface is almost vertical, *i.e.* the angle between the hydroxyl and the normal direction of surface is only 1.1°. Whereas, the hydroxyl group at the relaxed anatase(101) surface is tilted with the angle

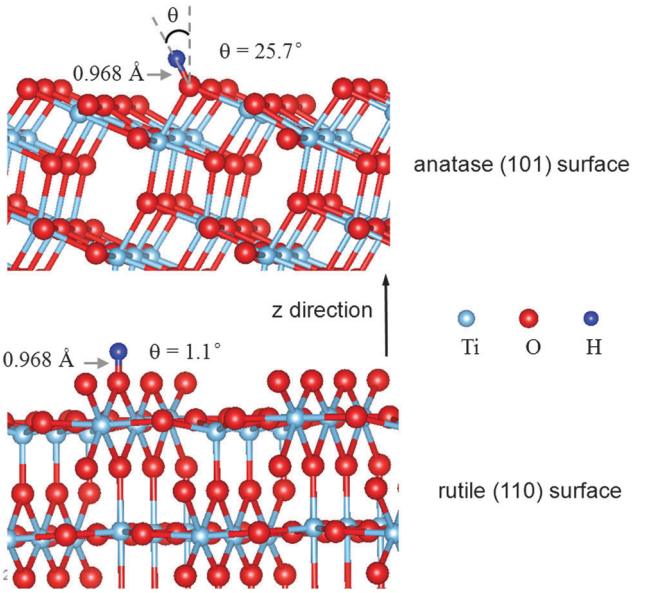

Fig. 4 The configurations of the hydroxyl groups at the anatase(101) and rutile(110) surfaces.

of 25.7°. Taking the dipole moment of O–H (p_{O-H} = 0.32 e Å) estimated from the dipole moment of a water molecule,[25] the projection of p_{O-H} to the normal direction is determined to be 0.28 and 0.32 e Å for the anatase(101) and rutile(110) surfaces, respectively, which is in good agreement with Δp_z (0.27 and 0.38 e Å) obtained by our DFT+U calculations. This agreement supports the fact that the dipole moment of polar groups adsorbed onto surfaces is an important source to tune electron energies in TiO_2 and the energy band alignment between different TiO_2 phases.

To further examine the effect of higher defect coverage on the band alignment type, the rutile(110) and anatase(101) TiO_2 surfaces with the 1/3, 2/3, and 1 monolayer hydroxyl coverages have also been calculated. The obtained dipole moment is linearly proportional to the hydroxyl coverage, which is always larger for the rutile surface than the anatase one at the same coverage. Considering eqn (1), the band edges of the rutile(110) surface always surpass those of the anatase(101) surface upon the same extent of hydroxylation from 1/6 ML to 1 ML, maintaining the staggered type alignment.

The O–Hs and O-vacs introduce positive Δp_z values onto TiO_2 surfaces. Then an interesting question arises what will happen if a negative Δp_z is introduced. This supposition can be tested through adsorption of fluorine onto the rutile(110) and anatase(101) TiO_2 surfaces. The fluorine atom has a great electronegativity value and readily forms polar covalent bonds with an under-coordination Ti atom.[45,46] Our calculation finds that in this case electron energies in the rutile TiO_2 decrease more than that in the anatase TiO_2, then the reverse straggled type (*i.e.* band edges of anatase are higher than those of rutile) may take place, as illustrated in the last column of Fig. 3. Negative Δp_z values are introduced with the values of −0.51 e Å and −0.68 e Å for the anatase(101) and rutile(110) surfaces respectively when U = 4.3.

Table 1 The difference in the total energy between the surfaces with and without defects, in units of eV, ΔE(defect), calculated using the DFT+U method

	U = 3.3 eV		U = 4.3 eV		U = 5.3 eV	
Surface	(101)	(110)	(101)	(110)	(101)	(110)
$\Delta\Delta E$(O–H)	−3.40	−3.69	−3.60	−3.86	−3.95	−4.16
ΔE(O-vac)	9.28	8.99	9.01	8.77	8.51	8.34
$\Delta\Delta E$(Ti–F)			−2.89	−3.51		

The above calculations have shown that the same defect coverage (1/6 monolayer of O–Hs or O-vacs) on the anatase(101) and rutile(110) surfaces can change the band alignment to staggered type. However, in practice, the two TiO_2 surfaces may have different defect coverages under the same preparation conditions. According to our DFT+U calculations, the rutile(110) surface favors the defects relative to the anatase(101) surface. As shown in Table 1, the energy increments from defects are lower for the rutile(110) surface than for the anatase(101) one, which will lead to different defect coverages in real materials.

In this sense, higher defect coverage on the rutile(110) surface can magnify the difference in Δp_z values between two phases of TiO_2, and further enhance the staggered type energy band alignment. Taking an extreme case, for example, for the rutile(110) surface covered with 1/6 monolayer O–H and the clean anatase(101) surface, the valence (conduction) band edge of rutile is higher for 0.73 (0.54) eV than that of anatase. Such significant energy spaces between the corresponding band edges for two TiO_2 phases were also observed by experiments. The polycrystalline anatase thin films and rutile single crystals prepared by Pfeifer *et al.* show that the VBM (CBM) of rutile is 0.7 (0.5) eV above that of anatase according to photoelectron spectroscopy analysis.[47]

It should be noted that the type of energy band alignment between rutile and anatase TiO_2 is also dependent on the measuring methods. Note that the (photo)electrochemical techniques derive the band edges from the flatband potential, where the band bending at the semiconductor–liquid interface is eliminated. So, unlike the photoelectron spectroscopy method, which measures the values of the energy-band shift arisen from the surface dipoles induced by defects, the electrochemical methods should give the same band edges of a semiconductor despite the surface band bending caused by defects. This is true as seen by the following evaluation. According to our DFT+U (U = 4.3 eV) calculations the mean value of energy-band shift per unit of the dipole moment for anatase (rutile) is 1.57 (1.65) eV e^{-1} $Å^{-1}$. And combined with data in Fig. 3, when the band bending caused by defects becomes completely flat, the conduction band edge of anatase is higher than that of rutile of 0.56 eV and 0.62 eV for surfaces with zero and 1/6 monolayer hydroxyl coverage respectively. In fact, in the electrochemical experiment conducted by Kavan *et al.*,[37] electrodes prepared from anatase crystals had the (101) face exposed, and were annealed in a hydrogen atmosphere at 500–600 °C to adsorb lots of hydroxyl groups,[48] and their impedance analysis established that the flatband potential of the anatase(101) surface is ∼0.2 eV higher than that of the rutile electrode prepared under the same conditions, lower than our estimated value of 0.62 eV from the ideal flatband potential. Thus the electrochemical methods did not give a staggered type of band alignment for rutile and anatase TiO_2 in the presence of defects at surfaces, rather a straddling type.

IV. Conclusion

The DFT+U calculations have shown that the energy band alignment for the perfect anatase(101) and rutile(110) surfaces is the straddling type, whereas the two surfaces with defects have the staggered band alignment. The common reductant defects O–Hs and O-vacs, as well as the oxidative defects Ti–Fs, prefer the staggered type band alignment. The switch of the band alignment from the straddling to staggered type is attributed to the electric dipoles induced by defects. Our computational results can provide a reasonable explanation to the long-standing debate on the energy band alignment for rutile and anatase TiO_2 and shed light on the electric-dipole effect tuning of photocatalytic activity.

Acknowledgements

This work was supported by the National Natural Science Foundation of China (Grant No. 51322206 and 11274060) and the Jiangsu Key Laboratory for Advanced Metallic Materials (Grant No. BM2007204).

References

1 A. Fujishima and K. Honda, *Nature*, 1972, **238**, 37–38.
2 O. Carp, C. L. Huisman and A. Reller, *Prog. Solid State Chem.*, 2004, **32**, 33–177.
3 L. Kavan, *Chem. Rec.*, 2012, **12**, 131–142.
4 T. L. Thompson and J. T. Yates, *Chem. Rev.*, 2006, **106**, 4428–4453.
5 Y. K. Kho, A. Iwase, W. Y. Teoh, L. Maedler, A. Kudo and R. Amal, *J. Phys. Chem. C*, 2010, **114**, 2821–2829.
6 G. Li, S. Ciston, Z. V. Saponjic, L. Chen, N. M. Dimitrijevic, T. Rajh and K. A. Gray, *J. Catal.*, 2008, **253**, 105–110.
7 Z. Liu, X. Zhang, S. Nishimoto, M. Jin, D. A. Tryk, T. Murakami and A. Fujishima, *Langmuir*, 2007, **23**, 10916–10919.
8 T. Ohno, K. Tokieda, S. Higashida and M. Matsumura, *Appl. Catal., A*, 2003, **244**, 383–391.
9 B. Sun, A. V. Vorontsov and P. G. Smirniotis, *Langmuir*, 2003, **19**, 3151–3156.
10 A. Zachariah, K. V. Baiju, S. Shukla, K. S. Deepa, J. James and K. G. K. Warrier, *J. Phys. Chem. C*, 2008, **112**, 11345–11356.
11 T. Kawahara, Y. Konishi, H. Tada, N. Tohge, J. Nishii and S. Ito, *Angew. Chem., Int. Ed.*, 2002, **41**, 2811–2813.
12 K. Komaguchi, H. Nakano, A. Araki and Y. Harima, *Chem. Phys. Lett.*, 2006, **428**, 338–342.
13 S. Shen, X. L. Wang, T. Chen, Z. C. Feng and C. Li, *J. Phys. Chem. C*, 2014, **118**, 12661–12668.

14 J. T. Carneiro, T. J. Savenije, J. A. Moulijn and G. Mul, *J. Phys. Chem. C*, 2011, **115**, 2211–2217.
15 D. C. Hurum, A. G. Agrios and K. A. Gray, *J. Phys. Chem. B*, 2003, **107**, 4545–4549.
16 Z. Luo, A. S. Poyraz, C. H. Kuo, R. Miao, Y. T. Meng, S. Y. Chen, T. Jiang, C. Wenos and S. L. Suib, *Chem. Mater.*, 2015, **27**, 6–17.
17 D. O. Scanlon, C. W. Dunnill, J. Buckeridge, S. A. Shevlin, A. J. Logsdail, S. M. Woodley, C. R. A. Catlow, M. J. Powell, R. G. Palgrave, I. P. Parkin, G. W. Watson, T. W. Keal, P. Sherwood, A. Walsh and A. A. Sokol, *Nat. Mater.*, 2013, **12**, 798–801.
18 J. Kang, F. Wu, S.-S. Li, J.-B. Xia and J. Li, *J. Phys. Chem. C*, 2012, **116**, 20765–20768.
19 P. Deak, B. Aradi and T. Frauenheim, *J. Phys. Chem. C*, 2011, **115**, 3443–3446.
20 J. C. Garcia, M. Nolan and N. A. Deskins, *J. Chem. Phys.*, 2015, **142**, 024708.
21 M. G. Ju, G. X. Sun, J. J. Wang, Q. Q. Meng and W. Z. Liang, *ACS Appl. Mater. Interfaces*, 2014, **6**, 12885–12892.
22 P. W. Peacock and J. Robertson, *Phys. Rev. Lett.*, 2004, **92**, 057601.
23 O. Sharia, A. A. Demkov, G. Bersuker and B. H. Lee, *Phys. Rev. B: Condens. Matter Mater. Phys.*, 2007, **75**, 035306.
24 H. M. Zhang, Y. K. Weng, X. Y. Yao and S. Dong, *Phys. Rev. B: Condens. Matter Mater. Phys.*, 2015, **91**, 195145.
25 D. Y. Zhang, M. N. Yang and S. Dong, *J. Phys. Chem. C*, 2015, **119**, 1451–1456.
26 D. Y. Zhang, M. N. Yang and S. Dong, *RSC Adv.*, 2015, **5**, 35661–35666.
27 A. Calzolari, A. Ruini and A. Catellani, *J. Phys. Chem. C*, 2012, **116**, 17158–17163.
28 S. Y. Yang, D. Prendergast and J. B. Neaton, *Nano Lett.*, 2012, **12**, 383–388.
29 P. E. Blochl, *Phys. Rev. B: Condens. Matter Mater. Phys.*, 1994, **50**, 17953–17979.
30 G. Kresse and J. Furthmuller, *Phys. Rev. B: Condens. Matter Mater. Phys.*, 1996, **54**, 11169–11186.
31 S. L. Dudarev, G. A. Botton, S. Y. Savrasov, C. J. Humphreys and A. P. Sutton, *Phys. Rev. B: Condens. Matter Mater. Phys.*, 1998, **57**, 1505–1509.
32 U. Diebold, *Surf. Sci. Rep.*, 2003, **48**, 53–229.
33 A. Klein, *Thin Solid Films*, 2012, **520**, 3721–3728.
34 A. Walsh and K. T. Butler, *Acc. Chem. Res.*, 2014, **47**, 364–372.
35 M. Peressi, N. Binggeli and A. Baldereschi, *J. Phys. D: Appl. Phys.*, 1998, **31**, 1273–1299.
36 Y. Q. Gai, J. B. Li, S. S. Li, J. B. Xia and S. H. Wei, *Phys. Rev. Lett.*, 2009, **102**, 036402.
37 L. Kavan, M. Gratzel, S. E. Gilbert, C. Klemenz and H. J. Scheel, *J. Am. Chem. Soc.*, 1996, **118**, 6716–6723.
38 I. Grinberg, D. V. West, M. Torres, G. Y. Gou, D. M. Stein, L. Y. Wu, G. N. Chen, E. M. Gallo, A. R. Akbashev, P. K. Davies, J. E. Spanier and A. M. Rappe, *Nature*, 2013, **503**, 509–512.
39 L. Li, P. A. Salvador and G. S. Rohrer, *Nanoscale*, 2014, **6**, 24–42.
40 D. Tiwari and S. Dunn, *J. Mater. Sci.*, 2009, **44**, 5063–5079.
41 G. Riegel and J. R. Bolton, *J. Phys. Chem.*, 1995, **99**, 4215–4224.
42 X. B. Chen, L. Liu, P. Y. Yu and S. S. Mao, *Science*, 2011, **331**, 746–750.
43 P. M. Kowalski, B. Meyer and D. Marx, *Phys. Rev. B: Condens. Matter Mater. Phys.*, 2009, **79**, 115410.
44 W. Tang, E. Sanville and G. Henkelman, *J. Phys.: Condens. Matter*, 2009, **21**, 084204.
45 X. C. Ma, Y. Dai, M. Guo and B. B. Huang, *J. Phys. Chem. C*, 2013, **117**, 24496–24502.
46 H. G. Yang, C. H. Sun, S. Z. Qiao, J. Zou, G. Liu, S. C. Smith, H. M. Cheng and G. Q. Lu, *Nature*, 2008, **453**, 638–641.
47 V. Pfeifer, P. Erhart, S. Li, K. Rachut, J. Morasch, J. Broetz, P. Reckers, T. Mayer, S. Ruehle, A. Zaban, I. Mora Sero, J. Bisquert, W. Jaegermann and A. Klein, *J. Phys. Chem. Lett.*, 2013, **4**, 4182–4187.
48 X. B. Chen, L. Liu, Z. Liu, M. A. Marcus, W. C. Wang, N. A. Oyler, M. E. Grass, B. H. Mao, P. A. Glans, P. Y. Yu, J. H. Guo and S. S. Mao, *Sci. Rep.*, 2013, **3**, 1510.

